Single Crystal Growth and Transport Properties of $RCrSb_3$ (R= La, Ce, Nd)

Neetu Rani

A dissertation submitted for the partial fulfilment of MS dual degree in Science

Indian Institute of Science Education and Research Mohali
April 2019

Certificate of Examination

This is to certify that the dissertation titled **"Single Crystal Growth and Transport Properties of $RCrSb_3$ (R= La, Ce, Nd)"** submitted by **Neetu Rani** (Reg. No. MP16008) for the partial fulfillment of MS degree programme of the Institute, has been examined by the thesis committee duly appointed by the Institute. The committee finds the work done by the candidate satisfactory and recommends that the report be accepted.

Dr. J. Bagla Dr. S. Sinha Dr. Sanjeev Kumar
(Supervisor)

Dated: 26 April 2019

Declaration

The work presented in this dissertation has been carried out by me under the guidance of Dr. Chandra Shekhar in group of Prof. Claudia Felser at Max Planck Institute of Chemical Physics of Solid, Dresden which is locally supervised by Dr. Sanjeev Kumar at the Indian Institute of Science Education and Research, Mohali.

This work has not been submitted in part or in full for a degree, a diploma, or a fellowship to any other university or institute. Whenever contributions of others are involved, every effort is made to indicate this clearly, with due acknowledgement of collaborative research and discussions. This thesis is a bonafide record of original work done by me and all sources listed within have been detailed in the bibliography.

Neetu Rani
(Candidate)

Dated: 26 April 2019

In my capacity as the supervisor of the candidate's project work, I certify that the above statements by the candidate are true to the best of my knowledge.

Dr. Sanjeev Kumar
(Supervisor)

Acknowledgment

I want to express my heartfelt gratitude to my supervisor, Dr. Sanjeev Kumar for his guidance. He has helped me to learn the critical skills necessary as an independent researcher. I want to thank my thesis committee members for their valuable suggestions and feedback. I would like to say great thank to Prof. Claudia Felser for allowing me to work in best infrastructures and would also like to say thanks to Dr. Chandra Shekhar for providing me excellent guidance during my project at Max-Planck Institute of Chemical Physics of Solids, Dresden, Germany. I am fortunate to have all the members of Prof. Claudia′s group. I am very thankful to Dr. Nitesh Kumar who taught me precious methods in crystal growth, and helpful discussions on Weyl and Dirac semimetals. Special thanks to Praveen Vir for making me learn every little thing in the lab during my stay in Dresden. I also want to thank Parul di, Vivek, Satya, Yu Pan for having nice coffee gossips. I miss Aleena′s Hindi skill that entertains us a lot during stress days in a foreigner country. I have spent six wonderful months in Max Planck Institute of Chemical physics of Solid and have learned a lot from many events, talks, Summer School, group discussions at the department of solid state chemistry.

During my work at IISER Mohali, I had the pleasure of working with several project students Tanmoy Pandit, Lalit Yadav and Mamta Raturi. During the class period, I have many happy and joyful memories with my friends Pardeep Tanwar, Geeta Choudhary, Mahinshi Singla, Ravi kumar, Subhashree, Avinesh, Riyaz. I am fortunate to have friend Neelu Kaswan, Sudesh Boora, Anu, and others who were always there with me in thick and thins of life. Studying in the IISER Mohali gave me opportunities to work with outstanding researchers, postdocs, and students and great infrastructures for which I am very thankful to Institute.

Finally, I would like to acknowledge the people who mean a lot to me, my parents and my siblings Komal Lamba, Dinesh Lamba, Satish Kadian, Pardeep Kadian. I have no suitable words that can adequately describe their everlasting love for me. Thank you mummy-papa for showing faith in me and giving me the liberty to choose what I desired. Last and most important, I dedicate this thesis to my parents, without their unconditional support, this would not have become possible.

List of Figures

Abstract

Topological semimetals are new classes of quantum materials, which are characterized by surface states induced by the topology of the bulk band structure. We inspired from interesting phenomenon is shown by these materials on a bulk scale, i.e., high transport properties, quantum anomalies which may be further beneficial for many other applications.

Reason for choosing $RCrSb_3$ and SmSb is its a new class of magnetic material both for the study and for their possible use. The RX (R = Ce, Pr, Sm; X=Sb, Bi) family of materials display a very large magnetoresistance and non-trivial band topologies. In this thesis, I have used Flux method to grow single crystal and characterize with the help of EDX, XRD, and Laue diffraction.

The magnetization and transport measurements were taken from SQUID magnetometry and PPMS of Quantum design respectively. We have observed a very high valued anomalous hall effect in $RCrSb_3$ while a beautiful Subhnikov de Hass oscillations observed in SmSb. To achieve better understanding in term of band structure from oscillations in SmSb which are very helpful to resolve the electronic structure and orientation of the Fermi surfaces. The value of anomalous Hall conductivity is 1230 $\Omega^{-1}cm^{-1}$ for $LaCrSb_3$, 1590 $\Omega^{-1}cm^{-1}$ for $CeCrSb_3$, 2930 $\Omega^{-1}cm^{-1}$ for $NdCrSb_3$ respectively which is highest ever conductivity reported among any quasi 2D material. This high AHE arises from internal band structure as calculated from our analysis. To dig the root cause of this high AHE, we performed thermal hall which also shows anomalous behavior (high Seebeck coefficient), Combined electrical, thermoelectric measurements reveal that this high value of the AHE and ANE may arise from the same cause which is large net Berry curvature. For a better understanding of the result, we are collaborated with the theory group and waiting for ARPES results to comment further.

Contents

Chapter 1

Introduction

Dirac proposed, in 1928 the first successful collation of special theory of relativity and quantum mechanics, called the Dirac equation. Later on, H. Weyl introduced simplified version for explaining massless fermions with a definite chirality [Weyl 29]. In 1937, Ettore Majorana did a modification using real numbers, which represented a neutral particle that was its antiparticle. These developments have found significant application in modern physics. The Dirac equation is the fundamental equation describing relativistic electrons, and the Majorana equations are a candidate to describe neutrinos [Majorana 37]. The Dirac equation is also a central concept leading to topological phenomena like zero modes and anomalies in quantum field theories. The best-known example of this phenomena is in graphene, where the massless two-dimensional Dirac equation shows a linear momentum dispersion relation.

We are concerned about analogous physics in three-dimensional crystals having linearly dispersing fermionic excitations that are described by the massless 3D Relativistic equations. These solid-state realizations offer us a stage where predictions made by relativistic theories can be applied and some new phenomenon that exists only in a condensed matter context emerge like Fermi arc surface states at the boundary of the material.

"Weyl semimetal" (WSM) was introduced to describe a phase where the chemical potential is near at the Weyl nodes [Yan 17].The major physical properties of Weyl fermions, such as chiral anomaly [Adler 69]. Topological consequences of Weyl nodes started to be explored with the realization that Berry curvature plays a crucial role in determining the Hall effect [Karplus 54] [Haldane 88]. Discovery and prediction of two and three dimensions of topological insulators have led to an explosion of activity in the study of a topological aspect of the band structure [Fu 07].

Weyl and Dirac semimetals are 3D phases of matter with gapless electronic excitations that are protected by various symmetries. Motivated from transport properties of Weyl semimetals for example high carrier mobility, large positive transverse magnetoresistance, low charge carrier density, low effective mass, we plan to grow some similar compound which may or may not be Dirac or Weyl semimetals but shows identical phenomenon's. However, very few available tools to characterize Weyl semimetals through electrical transport, negative magnetoresistance is most commonly used [Armitage 18].

Metallic magnetism is always a fascinating source of surprises. The Inter-metallic alloys formed by combining the elements of the 4f metals and the 3d metals, Cr in $RCrSb_3$ present an exciting category of magnetic materials both for the study of their magnetic behavior and for their further possible applications [Inamdar 09].

This whole series has a nearly 2D structure with RSb and $CrSb_2$ layers pile up along the a axis [Choi 07]. Successive layers of such compound allow for the control of the magnetic aspect through the interlayer coupling. The anomalous magnetism found in $RCrSb_3$, and the interaction between the itinerant 3d electrons of Cr ion and the localized 4f moments from the lanthanide series kept increasing when we go from left to right in series.

Based on which lanthanide element we have chosen, $RCrSb_3$ has been found to have either a purely Ferro or anti-ferromagnetic phase or combination of both the phases. The anti-ferromagnetic order evolves from the ferromagnetic order as a result of the competition between R^{3+} and Cr^{3+} ions. The atomic radius decreases from La to Lu; it found that substitution of the more massive rare earth element in $RCrSb_3$ causes the structure of the compound to contract and resulting into change in the magnetic properties of the system.

1.1 Hall Effect

If we pass an electric current flows through a conductor in a magnetic field, there is a force exerted by the magnetic field in the transverse direction of charge carriers which tends to align them to one side of the conductor. As seen from our Fig 1.1., A accumulate of charge at the sides of the conductors will balance this magnetic force,

producing voltage drop between across the two sides of the conductor. The transverse measurable voltage is called the Hall effect after E. H. Hall who discovered it in 1879 [Hall 79].

1.1.1 Theory of Hall effect

Consider a rectangular bar-shaped conducting material of thickness t kept in XY plane. An electric field applied in X-direction and current "I" flow through the sample. Let us consider w is the width of the sample and t is the thickness of the sample; the relation gives the current density, $J_x = I/wt$
If the direction of the applied magnetic field is z-axis, then the Lorentz force moves the electron toward the y-direction. It leads to the accumulation of charge carriers at one side of the sample. This causes the transverse electric field E_y in the sample. This develops a voltage difference along the y-axis is known as Hall voltage V_H.
In steady state condition, the magnetic force balanced by the electric force. Mathematically we can express it as eE=evB
Where e = electron charge, E = the hall electric field developed, B = the applied magnetic field and v = the drift velocity of charge carriers. And the current I can be expressed as I = venA, so using all the above equation we get,

$$V_H = Ew = vBw = IB/net, \qquad V_H = R_H IB/t$$

So $R_H = 1/ne$ is hall coefficient which is different for different charge carriers. Hall voltage has a different sign for positive and negative charge carriers, and it has been used to study conduction details in semiconductors and other materials where we have multiple types of charge carriers [Armen 07].

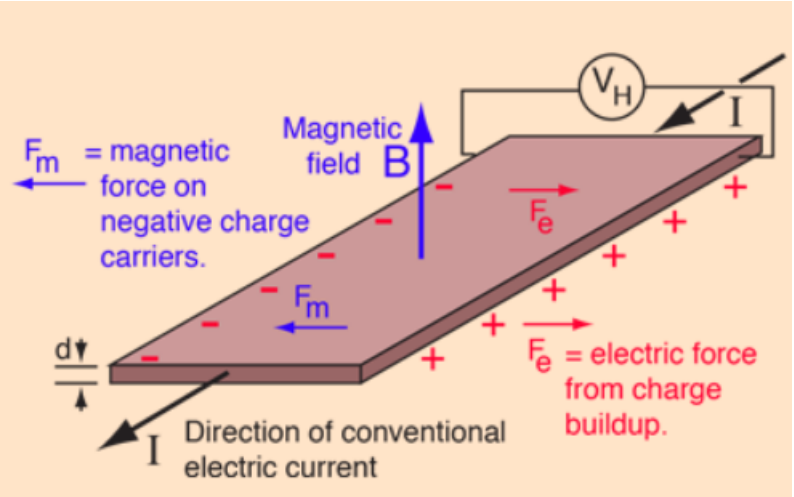

Figure 1.1: Hall Setup[Hal]

1.2 Berry Phase

The group velocity of electrons in the semiclassical limit is given as $v(k) = \nabla[E(k)]$. Karplus and Luttinger calculated that the position operator x in a periodic lattice fails to commute with itself.

$v(k) = \nabla[e(k)] - eEx\Omega(k)$, where $\Omega(k)$ is the "Berry curvature" terms. The extra term $eEx\Omega(k)$ is called the Luttinger anomalous velocity term. Topology is the study of spatial and geometrical properties which are intact by the continuous change of shape or size of figures. Topological invariant = quantity that does not change in constant deformation. A "Berry phase" is a phase angle (hopping from 0 and 2π) shows the global phase evolution of a complex vector carried around a path in its vector space. The concept was systematized in 1980 by Michael Berry. Berry curvature is often the largest at near-degeneracies [Shin 19].

1.3 Anomalous Hall Effect(AHE)

The anomalous Hall effect has intensive roots in the history of electricity and magnetism. E. Hall in 1879 discovered that when a current-carrying conductor placed in the presence of a magnetic field, the Lorentz force tries to moves its electrons against

one side of the conductor. Later, he reported that "moving electricity" effect was more dominating in ferromagnetic iron than other nonmagnetic conductors [Hall 81]. Hall effect discovered in ferromagnetic conductors is known as the anomalous Hall effect (AHE).

Karplus and Luttinger (KL) theory, The work of Karplus and Luttinger (KL) in 1954 was the first theory of the AHE which based on Bloch states [Karplus 54]. According to KL calculations, there is a significant role played by the existence of bands and the combined overlap of Bloch states. This theory ignores all lattice disorder, so the Hall effect it tells based on an intrinsic mechanism alone. In a ferromagnetic, through spin-orbit coupling (SOC) the orbital motion of the itinerant electrons couples to spin order. KL theory considers, the moments of the ferromagnetic state are itinerant, i.e., the electrons carrying the transport current also produce the magnetization. It recognized in the 1950s that if the magnetic polarization of system mingled with an orbital motion by SOC, Hall phenomenon should exist in ferromagnetic materials even in the absence of an external magnetic field.

Karplus and Luttinger pointed out the existence of an additional term in the velocity operator proportional to the gradient of electrical potential acting on the carriers which adds a term acting like magnetic field called Berry phase term. The Hall conductivity derived from this method is proportional to the Berry curvature summed over the occupied band. Based upon the system taken we can tune ferromagnetic polarization and SOC which is further related to Berry phase [Sinitsyn 07].

The measured Hall resistivity, ρ_{yx} of any magnetic material can be expressed in general from a relation as, $\rho_{yx} = \rho_{y_x}^{N} + \rho_{y_x}^{A} + \rho_{y_x}^{T}$,
Where, the normal Hall effect (NHE) is determined from the relation $\rho_{y_x}^{N} = R_0\mu_0 H$, and it is due to the Lorentz force. R_0 is the normal Hall coefficient and $\mu_0 H$ is the applied external magnetic field [Pugh 30]. R_0 is depend on the density of charge carriers.

The anomalous Hall effect (AHE) in a magnetic material is given by the $\rho_{y_x}^{A} = (\ \alpha\rho_{xx} + S_A\rho_{x_x}^{2})\mathrm{M}$, Where α and S_A corresponds to the extrinsic contribution from skew scattering and the impurity density independent contributions, respectively. M is the magnetization and ρ_{xx} is the longitudinal resistivity [Berger 70]. The intrinsic AHE originates from the momentum space Berry curvature, which is measured in the

high field polarized regime. If $\rho_{x_y}^{A}$ and $\rho_{x_x}^{\alpha}$ were plotted, where α is the scaling power factor $\alpha = 2$ is for the intrinsic KL mechanism and the extrinsic side-jump mechanism and $\alpha = 1$ is for another extrinsic skew-scattering mechanism [Kooi 54].
Lastly, $\rho_{y_x}^{T}$ is the topological Hall resistivity which arises due to any noncoplanar order of spins.
So in summary one can understand AHE as follow:

1. When $\sigma_{y_x}^{A}$ is independent of σ_{xx}, the AHE can grasp in terms of the geometric concepts of Berry phase in momentum space [Chang 96]. The anomalous Hall current can be thought of as the unquantized version of the quantum Hall effect, while in 2D systems the intrinsic AHE is quantized in units of e^2/h at temperature T=0.

2. Three section have been identified from large body of experimental data for diverse materials:(i) a high conductivity regime $[\sigma_{xx} > 10^6(\Omega cm)^{-1}]$ in which a linear contribution to $\sigma_{y_x}^{A} \sim \sigma_{xx}$ due to skew scattering dominates. (ii) is an intrinsic or scattering-independent regime in which $\sigma_{y_x}^{A}$ is roughly independent of σ_{xx} $(10^4(\Omega cm)^{-1} < \sigma_{xx} < 10^6(\Omega cm)^{-1})$ (iii) a bad metal regime$(\sigma_{xx} < 10^4(\Omega cm)^{-1})$ in which $\sigma_{y_x}^{A}$ decreases with decreasing σ_{xx} at a rate faster than linear.

3. The intrinsic mechanisms studied in materials having a strong SOC, like oxides and magnetic semiconductors.

Chapter 2

Materials and Crystal Growth Method

2.1 Raw material for crystal growth

Single crystals of $RCrSb_3$ (R = La, Ce, Nd, Gd) were grown by solution growth method (Flux) using Sb as a flux in Box furnace. For synthesis La, Ce, Nd polished pieces (La, Ce, Nd pieces, 99.9 %), Chromium(Cr pieces, 99.99% pure), and Antimony (Sb pieces, 99.999 % pure) were used.

2.2 Poly and Single Crystal

The first scientific approach of crystal growth began in 1611 when Kepler concluded that snow crystals built by closed packed spherical particles and posed, in such a way, the correct principle of crystallographic form, followed by Nicolous Steno, who explained the origin of various external forms [Bohm 85].

Crystal growth is a field that demands the collaboration of experts from various fields. The importance of rareness of single crystals related to their symmetry, molecular structure, purity, and the physicochemical environment of their formation. It is a procedure of arranging atoms, ions, molecules into regular 3D periodic arrays. However, in reality, crystals are never perfect due to the presence of various local disorder and dislocations.Therefore crystal grower have to produce perfect single crystals of the required shape, size and characterize them to understand their purity and quality. It is an important branch of materials science for the formation of technologically

important materials of different shapes and size.

2.2.1 Why we need single crystal?

Single crystal maintains transnational symmetry over macroscopic distance. We should grow single crystal because structure determination and intrinsic property measurements are preferably, sometimes exclusively, carried out on single crystals. For specific applications, we rely on optical and electronic properties (laser crystals, semiconductors, etc.); for that single crystals are necessary.

2.2.2 Theories of Crystal Growth

Crystal growth is the chemical process of having solid, liquid or gas to form a homogeneous solid substance having 3D atomic arrangement. From an initially disordered phase, three basic steps involved in the formation of crystals are:
1. Supersaturation or super-cooling.
2. Nucleation
3. Growth of the nuclei into single crystals.

Nucleation or crystallization is an essential part of crystal growth. Steady-state super-cooling maintained during crystal growth to obtain the higher-quality crystal. Sometimes nucleation may occur spontaneously due to the condition in the parent phase, or it induced artificially [Cahn 60]. Gibbs was the first to explain the formation of small embryonic clusters of some critical size is a prerequisite for the development of a macroscopic crystal.

2.2.3 Crystal Growth Techniques

There is the various method of crystal growth, but we will mainly discuss only those which involved in inorganic crystal growth.

Self-Flux Growth Method

The single crystal growth method, we have used during my MS thesis is the self-flux growth method. In the usual flux method, or solution growth method, the target material is dissolved in a solvent to super-saturation, and the temperature is lowered,

and dissolved material crystallizes out of the solvent. In the self-flux method, one of the starting material itself acts as the flux in which the target material is grown. In this process, one starts with an off-stoichiometric amount of starting materials with an excess of the component which is going to be used as the flux. A mixture of starting materials is heated to a temperature which is higher than the melting point of the flux, and then the mixture is cooled slowly (around 1–5 $°C$/hr). Crystals grow during this slow cooling stage.

Due to the long duration of the growth process the choice of crucible material is essential. The crucible should be made of highly stable, non-reactive material which has high thermal conductivity. The crucibles most commonly used are ceramics such as alumina (Al_2O_3), zirconia (ZrO_2), silicon carbide (SiC), and boron nitride (BN). The other main challenge in the flux growth method is to separate the crystal from the flux. The common methods used to remove flux from the crystals is to either decant the flux while it is still molten or to dissolve the flux in some suitable solvent which doesn't attack the crystals themselves [Dhanaraj 10].

1. Solid–Solid	Solid	T →	Solid Devitrification Strain annealing Polymorphic phase change Precipitation from solid solution
2. Liquid–Solid			
i) Melt growth	Molten material	Dec. T →	Crystal Bridgman–Stockbarger Kyropoulos Czochralski Zoning Verneuil
ii) Flux growth	Solid(s) + Flux agent(s)	Dec. T →	Crystal(s)
iii) Solution growth	Solid(s) + Solvent	Low T →	Crystal(s) Evaporation Slow cooling Boiling solutions
iv) Hydrothermal growth	Solid(s) + Solvent	High T → High p	Crystal(s) Hydrothermal sintering Hydrothermal reactions Normal temperature gradient Reversed temperature gradient
3. Gas–Solid	Vapor(s)	→	Solid Sublimation–condensation Sputtering Epitaxial processes Ion-implantation

Figure 2.1: From above figure we may get idea about the all methods that we have: High temperature methods($1500°C$ >):- Czochralski, Stockbarger and Bridgman, Verneuil, Zone melting.Medium temperature methods:- Fluxes, Electrochemical from melts, Hydrothermal. Vapor phase transfer.Low temperature methods Sublimation:- Solution Gel [Dhanaraj 10].

2.3 Glove box

Sometimes samples are very sensitive towards oxygen, and if it is the case, then It is essential to preserve the grown samples from the exposure to the unwanted impurities, gases in the atmosphere and sunlight. The Glove Box is always filled with high purity Argon gas. Since a slight degradation of the sample can change the physical properties. To avoid any contamination from the ambient environment, we have kept our samples in Glove Box manufactured by mbraun as shown in Fig 2.2

Figure 2.2: Glove Box

2.4 Box furnace for single crystal growth

We use high-temperature box furnace, manufactured by Nabertherm, Germany for crystal growths. It has 4 SiC heating elements and can go up to a temperature as high as 1400°C. Box Furnaces only process products one at a time or in a single group. A Box Furnace features a vertical lift or swings outdoor allowing the various sized products to be placed in the furnace.

Figure 2.3: Box Furnance

2.5 Energy Dispersive X-ray spectroscopy

Electron dispersive X-ray (EDX) measurements performed at 25keV and 30keV energy. From the EDX measurements, the stoichiometry of the compound confirmed. Electron matter interaction generates a variety of signals which has various information about the sample (Figure 2.4). Backscattered electrons produce images with contrast that carries information on the differences in atomic number; secondary electrons give topographic information; cathodoluminescence tell us about the electronic structure and the chemical composition of materials, and transmitted electrons can describe the sample's inner structure and crystallography.

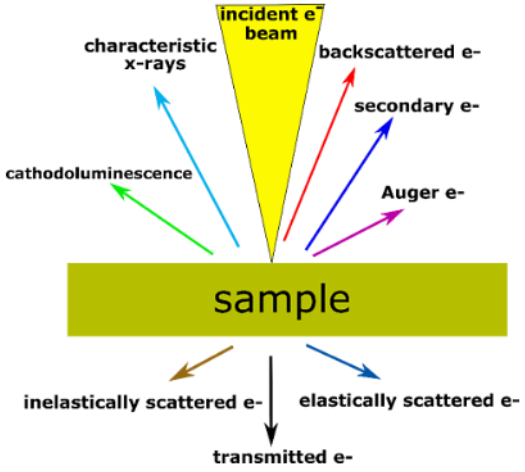

Figure 2.4: Illustration of the electron-matter interaction showing its different products [EDX].

EDX analysis in SEM:- When the electron beam hits the sample and transfers its part of the energy to the atoms of the sample, the electron of an atom use this energy to go into higher energy shell or be knocked-off from the atom. In this kind of transition, the electron leaves behind a hole of positive charge and, in the second step of the process, It attracts the negative charge electrons from higher-energy shells.

When an electron from such a higher-energy shell falls into the hole of lower-energy, the difference in energy can be released in the form of an X-ray. This X-ray has a particular wavelength related to the energy difference between these two shells [Jenkins 95].

2.6 Wire Saw for shaping Crystals

Cutting technique that used for precision guidance and consistent application of a material. Cutting should be in such a way that do not introduce deformations (eliminate the part "or defects"), minimal loss of material from cutting, wire diameters from 20μm to 60μm. Wire saws are ideal for the precise cutting of materials in Solids.

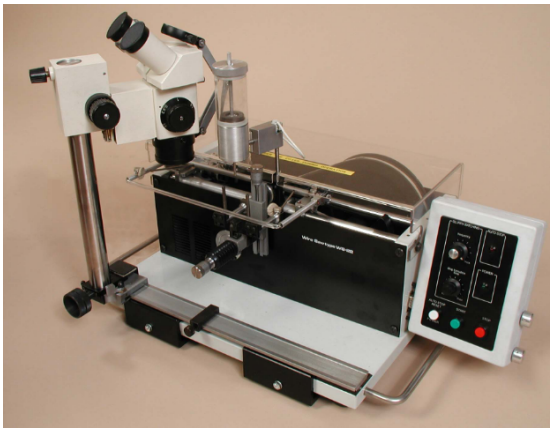

Figure 2.5: Wire saw for shaping crystals

2.7 Laue Diffraction

Laue diffraction is often used for mounting single crystals in a known orientation, for example for polishing a surface or for doing measurements. Continuous radiation with all possible wavelengths that Max von Laue used to clash on a stationary crystal. Through this process, the crystal generates a set of diffracted beams that

related to the symmetry of the single crystal. From Bragg's reflection law, constants like the inter-planar spacing's (d)and the crystal position referred to the incident beam. Wavelength λ and integer numbers n are variables. The diffraction pattern will consisting of (for the same spacing d) first order of diffraction (n=1) of a certain wavelength, the second order (n=2) of half the wavelength ($\lambda/2$), the third order (n=3) with wavelength $\lambda/3$, etc [Hammond 01].

Laue diagram is a stereographic projection of the crystal. Two types of geometrical methods are possible for Laue, depending on the crystal position concerning the photographic plate: reflection or transmission. Laue diffraction is two types:- Back Scattered Laue-in this type of Laue photographic plate is placed in-between the crystal and X-rays. The beams diffracted in backward diffraction recorded on film. Transmission Laue- in this type of Laue photographic plate is placed behind the crystal to record the beams which pass through the crystal as seen from Fig. 2.6

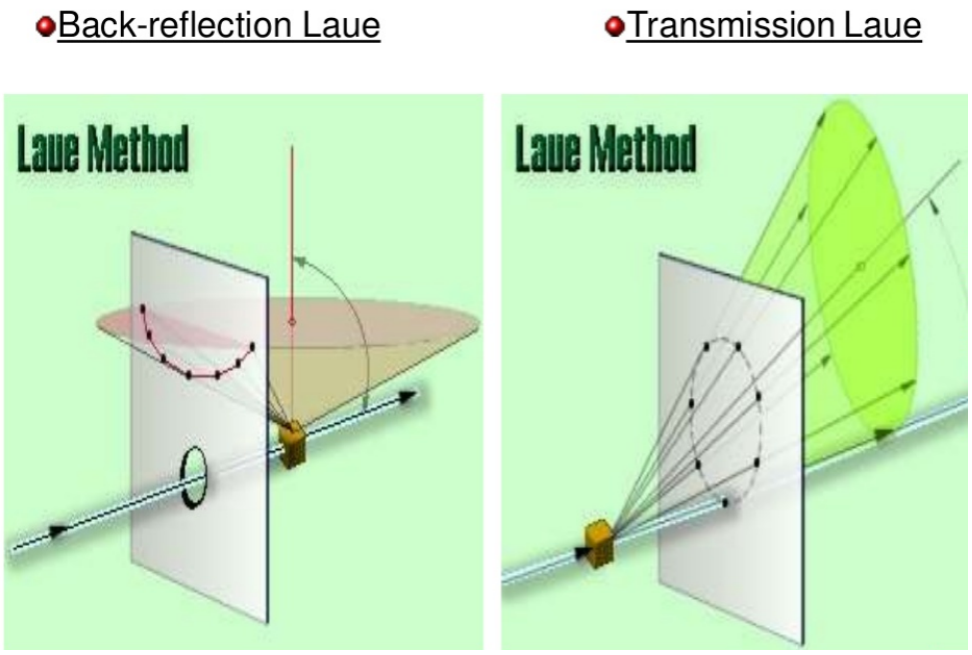

Figure 2.6: Laue diffraction setup[Lau]

2.8 Physical Properties Measurement System (PPMS)

The PPMS is low-temperature and magnet system for the measurement of material properties like specific heat, magnetic susceptibility, electrical and thermal transport features. PPMS represents a unique steup in laboratory equipment: variable

temperature-field system, designed to perform a variety of automated measurements. Sample environment controls include fields up to ±16 tesla and temperature range of 1.9 - 400 K.

Figure 2.7: PPMS system

2.9 Superconducting Quantum Interference Device (SQUID)

The superconducting quantum interference device (SQUID) is including insulating layers between two superconductors to form two parallel Josephson junctions. The device is shaped as a magnetometer to detect incredibly small magnetic fields. The

high sensitivity of the SQUID devices is related to measuring changes in the magnetic field associated with one flux quantum. One of the discoveries associated with Josephson junctions was that flux is quantized in units.

Figure 2.8: SQUID

Chapter 3

Characterization and Electric Transport Measurements

During my MS work I had grown many single crystals including $EuAs_2Sn_2$, SmSb, GdPtBi, NdPtBi, $LaCrSb_3$, $CeCrSb_3$, $GdCrSb3_3$, $NdCrSb_3$ but our main focus will lies on SmSb and $RCrSb_3$ series.

3.1 SmSb

X (Sb,Bi) (X = Lanthanide) series of semimetals with a cubic rock salt structure. These materials are commonly found to have an extremely large magnetoresistance [Tafti 16] [Li 96]. The RX (R = Ce, Pr, Sm; X=Sb, Bi) family of materials display a very large magnetoresistance and non-trivial band topologies and SmSb is antiferromagnetic semimetal.

3.1.1 Laue diffraction

Single crystals of SmSb were grown by solution growth method (Flux) using Sb as flux. For synthesis, high purity Samarium polished pieces (Sm pieces, 99.9 % pure), and Antimony (Sb pieces, 99.999 % pure) were used. Quantum oscillations are generally studied to resolve the electronic structure. To achieve better understanding in term of band structure, we probe Shubnikov–de Haas oscillations in SmSb.

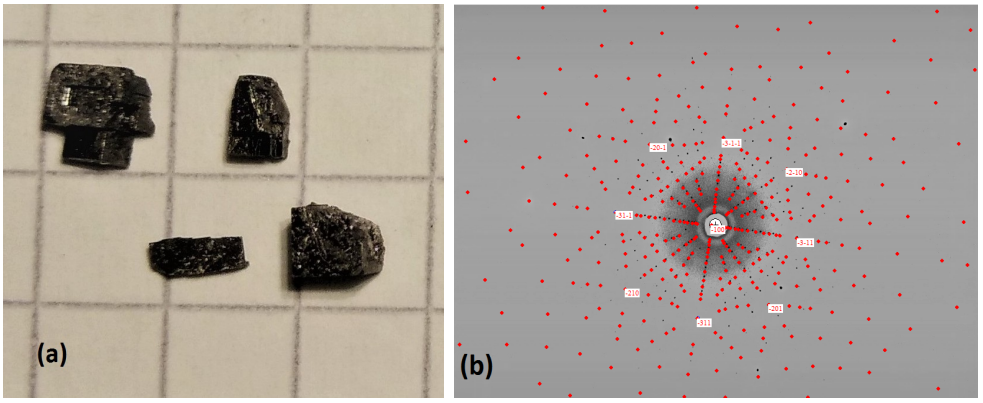

Figure 3.1: (a) image shows single crystal of SmSb and 3.1b shows refined image of SmSb from Laue diffraction.

3.1.2 Shubnikov de Hass oscillations

The quantum oscillation effect was first discovered by W. Haas and P. van Alphen when measuring magnetization, and by L. Shubnikov and de Haas when measuring magnetoresistance in Leiden in 1930. During the study of the single crystal of bismuth, oscillatory variations in the magnetization and longitudinal resistance with the magnetic field observed. In 1952 L. Onsager gave a theoretical explanation of quantum oscillations [Onsager 52], and a quantitative theory by Lifshitz and Kosevich in 1955. A significant theoretical advance was made at this time by Dingle (1952b), who pointed out that electron scattering should broaden the Landau levels and that this should lead to an extra amplitude reduction factor, which gives rise in temperature called Dingle temperature T_D [Dingle 52].

In the 1960s, Schoenberg revealed the richness and deep essence of the quantum oscillation effect [Shoenberg 09]. When a 3D noninteracting electron gas placed in magnetic field H_Z, we get quantized energy levels $E_N = h\omega(N + 1/2)$ in the K_x, k_y plane. There is a continuous spectrum along the magnetic field direction where N=0,1,2,... is the Landau level number and ω is cyclotron frequency.

The Onsager idea based on the simple semi-classical treatment of how electrons move in a magnetic field and it appears that the dHvA frequency F (i.e., the reciprocal of the period in l/H) is directly proportional to the extremal cross-sectional area A of the Fermi surface.

The relation is given by F = (ch/2ne)A

For transport measurements, the crystal aligned using Laue diffraction and then cut into the rectangular bar-shaped sample using a wire saw. Contact on samples was made using Platinum wire of 25mm diameter.

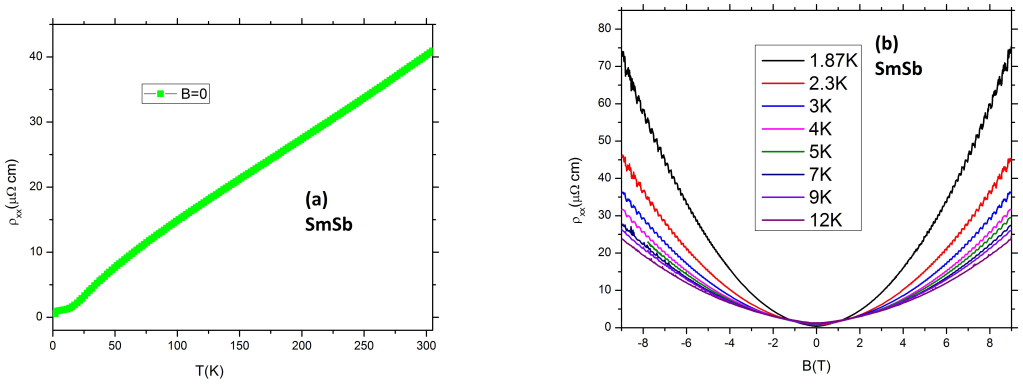

Figure 3.2: Resistivity vs. temperature of SmSb at zero field shown in fig. 3.2a while fig. 3.2b shows resistivity at various applied magnetic field and temperature

We can easily see in low temperature Transport resistivity shows oscillation in its value.

3.1.3 Calculations:-

A quantitative analysis of the SdH oscillations can be made using the Lifshitz-Kosevich (LK) equation which is given by [Lifshitz 58]:- $\Delta R \propto R_T R_D cos(2\pi[F/B-(1/2-\phi)])$ Where, $R_D = exp(-\lambda T_D)$ is the Dingle factor, T_D is the Dingle temperature, the temperature dependent damping of the oscillations is given by the factor $R_T = \lambda T/sinh(\lambda T)$, with $\lambda = (2\pi^2 K_B m*/eB)$ and m$*$ the effective cyclotron mass, K_B is Planks constant, e is charge of electron and B is applied magnetic field. The phase $\phi = (\phi_B/2\pi) - \delta$, where ϕ_B is the Berry phase and δ is an extra phase factor. The value of this additional phase shift δ depends on the dimensionality of the Fermi surface and takes the value 0 or $\pm 1/8$ ($\mp$for electron like and for the hole like) for two and three dimension, respectively.

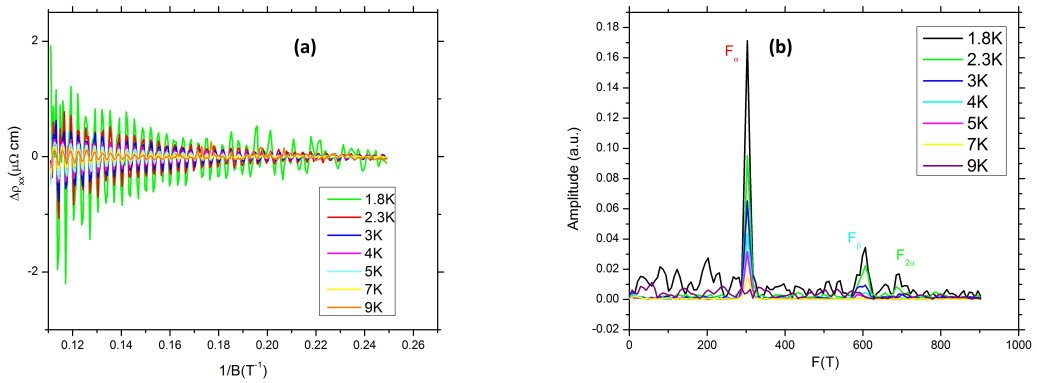

Figure 3.3: After smooth background subtraction from ρ_{xx} to reveal resistivity oscillations that are clearly visible and periodic in $1/B$ as seen from fig.3.3a while Fourier transform of 3.3a shown in figure 3.3b for evaluating particular frequency of oscillations.

The damping factors R_T from LK fit can be used to calculate important band parameters such m$*$, while by fitting field dependent damping of the oscillation amplitude with $R_D = exp(-\lambda T_D)$, we calculate the Dingle temperature of R_D= 2.71K and from R_D we can determine lifetime τ and mobility μ of the carriers. Mass of electron calculated from both curve fitting of fig. 3.4 is 0.40513 m_e and 0.5513 m_e for alpha and beta band respectively.

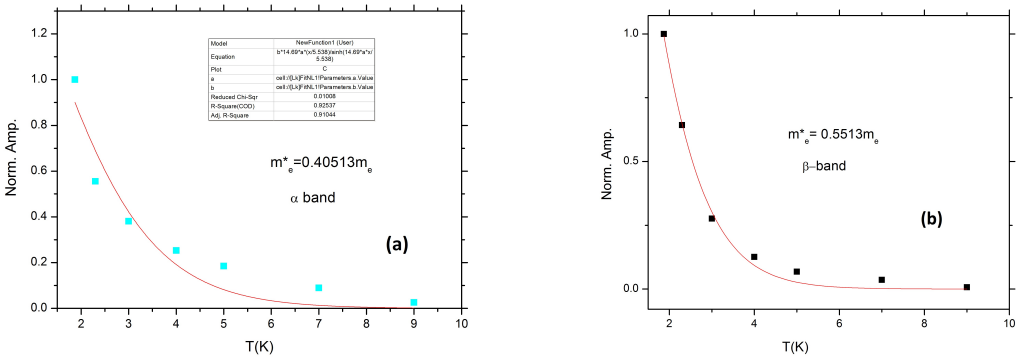

Figure 3.4: Shows LK fit of alpha and beta band in 3.4a, 3.4b respectively.

3.1.4 Conclusion

To construct the Landau level fan diagram, we assign the landau index n to the minima of quantum oscillations as displayed in Fig. 3.3 And fitting F/B-$(1/2-\phi)$ with linear fit, intercept gives us $\phi = (\phi B/2\pi) - \delta$, Which is directly related to Berry phase. And the fit is called Landau Fan diagram as shown in fig. (3.5) Since the lowest observed Landau index is 34 in the 9T measurements, the uncertainty associated with the fitted intercept is large, indicating that the determination of the Berry phase is not reliable.

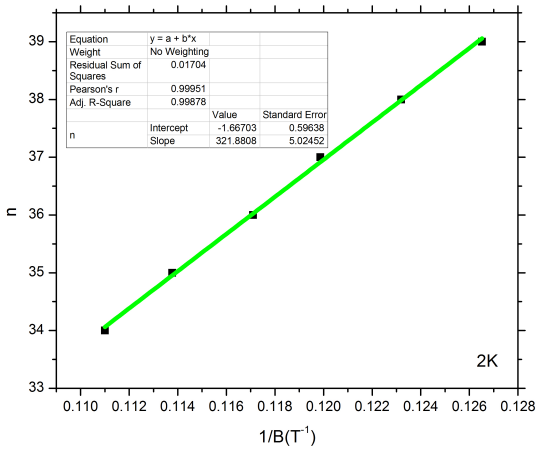

Figure 3.5: Landau Fan diagram

3.2 $RCrSb_3$

Magnetization, electrical resistivity performed on single crystal $RCrSb_3$ (R=La,Ce,Nd) samples [Raju 98].

$RCrSb_3$ layered material, crystallizes in space group Pbcm with a= 13.266Å, b= 6.188Å, and c = 6.100Å at 293K as determined by neutron diffraction [Granado 01]. At low temperatures, the resistivity follows a T^2 law with an inflection point at about 125K, above which a weaker temperature dependence. Magnetization measurements also indicate a phase transition at 125K of apparently ferromagnetic nature. These properties are indicative of itinerant electron ferromagnetic behavior arising from strong electron correlation in the Cr-d bands [Shim 04].

3.2.1 Single Crystal growth

Single crystals of $RCrSb_3$ (R = La, Ce, Nd, Gd) were grown by solution growth method (Flux) using Sb as flux. For synthesis Lanthanum, Gadolinium polished pieces (La, Gd pieces, 99.9 %), Chromium(Cr pieces, 99.99 %), and Antimony (Sb pieces, 99.999 %) loaded in an alumina crucible in a molar ratio of 1:1:10 and sealed in an evacuated quartz tube under 3-bar partial pressure of argon.

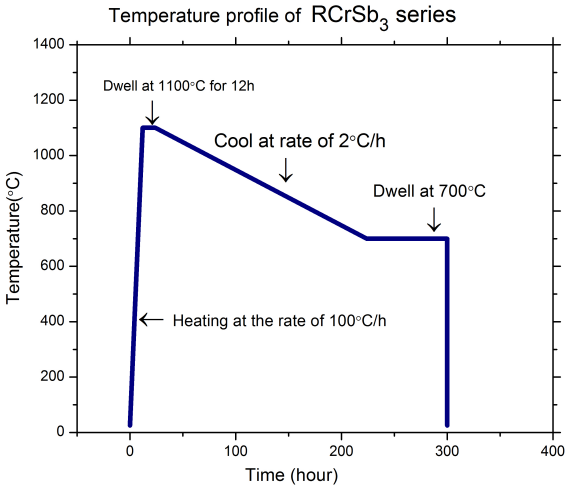

Figure 3.6: Synthesis route for $RCrSb_3$ series i.e.tube heated at a rate of 100K/h up to 1100 K and left for 12h at this temperature. For the single crystal growth, the temperature reduced at a rate of 2K/h to 700K, and the extra Sb flux was removed by decanting from the ampoule at 700K.

Similarly $CeCrSb_3$ and $NdCrSb_3$ single crystal were grown using same methods as mentioned above with a bit different molar ratio i.e. 1:1:12, 1:2:20 respectively. We obtain crystals, 4-10 mm in size, with a preferred growth orientation along [100], as confirmed by Laue diffraction. The composition and structure were checked by energy-dispersive X-ray analysis and Laue X-ray diffraction respectively. For transport measurements, the crystal was aligned along the [010], [001]-direction using Laue diffraction and then cut into a bar-shaped sample using a wire saw.

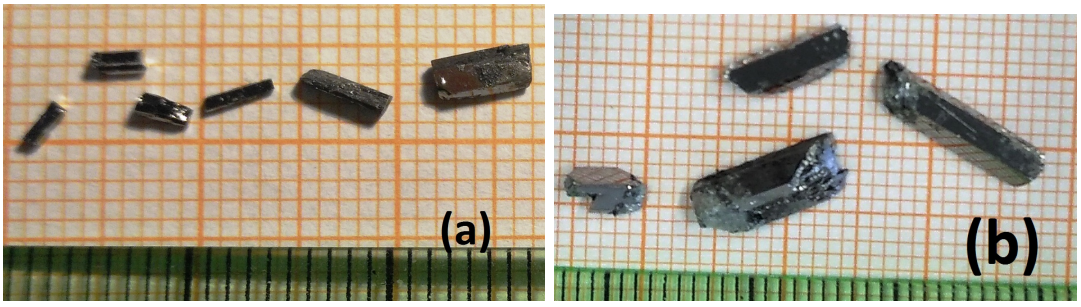

Figure 3.7: Single crystal of $LaCrSb_3$ and $NdCrSb_3$ of size 5-9mm in fig. 3.7a and 3.7b respectively.

3.2.2 EDX

EDX measurements were done at 25keV energy. Before doing EDX on materials we cleaved its surface using Scotch tape, and then EDX was done.

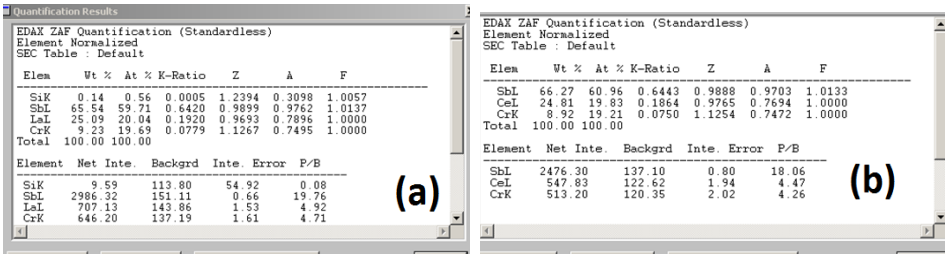

Figure 3.8: (a)image shows chemical composition of $LaCrSb_3$ while fig. 3.8b shows chemical composition of $CeCrSb_3$ extracted from EDX.

3.2.3 Laue Diffraction

In crystallography, from the process of diffraction by crystal lattice, the Laue equations relate the incoming waves to the outgoing waves, and we will get to know about the crystal orientation from it.

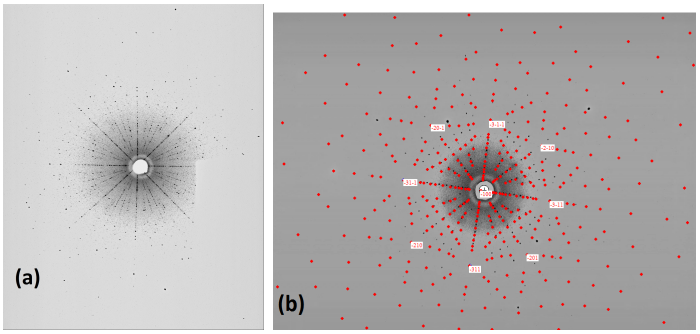

Figure 3.9: (a) shows raw Laue image of $LaCrSb_3$ and 3.9b shows refined image of 3.8a

3.2.4 Magnetization

Magnetic measurements were performed using quantum design superconducting quantum interference device (SQUID).

$LaCrSb_3$

$LaCrSb_3$ is found to have FM transition at $T_C = 132K$. A surprising property of this system is the presence of an apparent AFM transition whose Neel temperature (T_N = 98 K) is less than the Curie temperature (T_C = 132 K). Neel transition suppressed with small magnetic field 250G, magnetic transitions are due to the 3d electrons of Cr. We observed magnetization of $LaCrSb_3$ along each direction individually as shown in below figures.

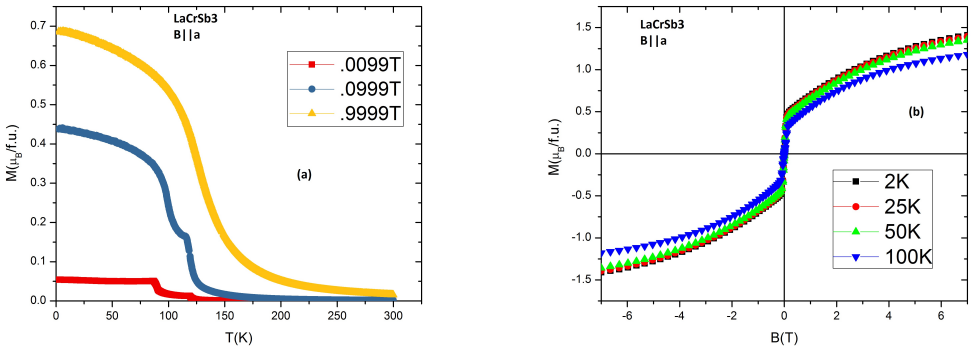

Figure 3.10: (a) shows M vs.T at different B while 3.10b shows M vs. applied field.

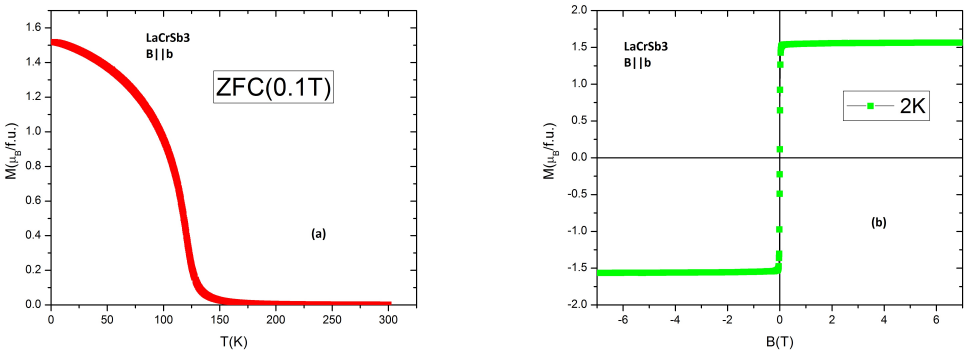

Figure 3.11: (a) shows M vs.T while 3.11b shows M vs. applied field

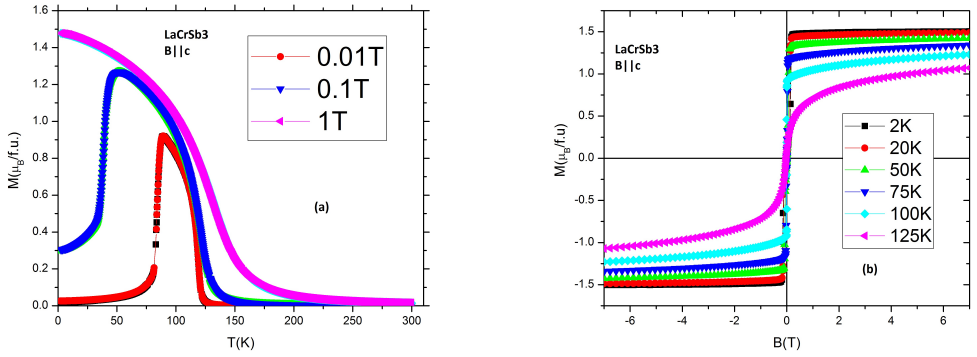

Figure 3.12: (a) shows M vs.T at different B while 3.12b shows M vs. applied field.

$CeCrSb_3$ and $NdCrSb_3$

The saturation moment of $CeCrSb_3$ along the c axis is $3.28\mu_B$/ f.u., and along the b axis, the magnetization saturates to $1.29\mu_B$/ f.u. as seen from fig. 3.13a, similarly in figure 3.13b at 107.8 K, ferromagnetic ordering of the Cr moments of $NdCrSb_3$ occurs; at 12.7 K, ferromagnetic order of the Nd and Cr moments occurs [Inamdar 08]. Both ferromagnetic ordering transitions in $NdCrSb_3$ are manifested as kinks in the temperature dependence of the electrical resistivity.

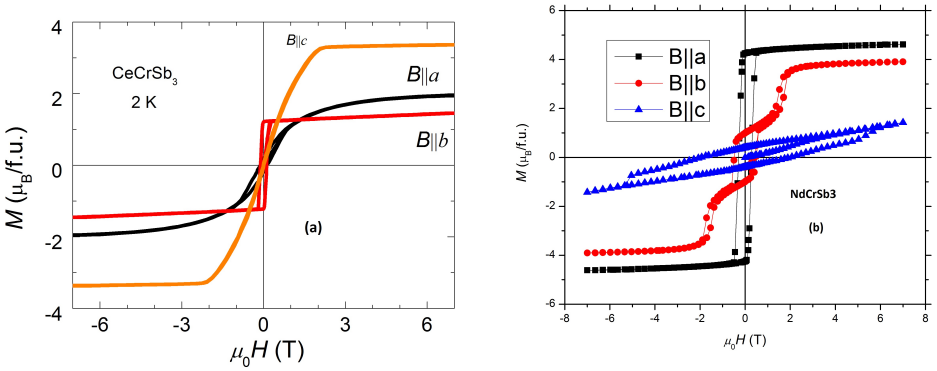

Figure 3.13: Magnetization vs. applied B of $CeCrSb_3$, $NdCrSb_3$ at 2K along all three direction shows in Fig. 3.12a, 3.12b respectively.

3.2.5 Electric Transport Measurements

Transport measurement was performed using the Physical Property Measurement System (PPMS Quantum Design). For transport measurements, the crystals were aligned along the [010], [001] direction using Laue diffraction and then cut into the rectangular bar-shaped sample using a wire saw. Contact on samples was made using Platinum wire of 25mm diameter.

$LaCrSb_3$

Resistivity data indicate metallic behavior. Hall measurement of $LaCrSb_3$ is shown in the figure 3.15a along B $\parallel$ b while insects in fig. 3.15a show Hall measurement along B $\parallel$ to c and a axis. As clearly seen from measurement we observe high anomalous hall in both b and c direction, right image shows conductivity vs. applied magnetic field B at various temperature calculated from hall measurement using the formula $\sigma_{yx} = \rho_{yx}/(\rho_{xx}^2 + \rho_{yx}^2)$ and found that maximum hall conductivity is 1230 $\Omega^{-1}cm^{-1}$ along b direction.

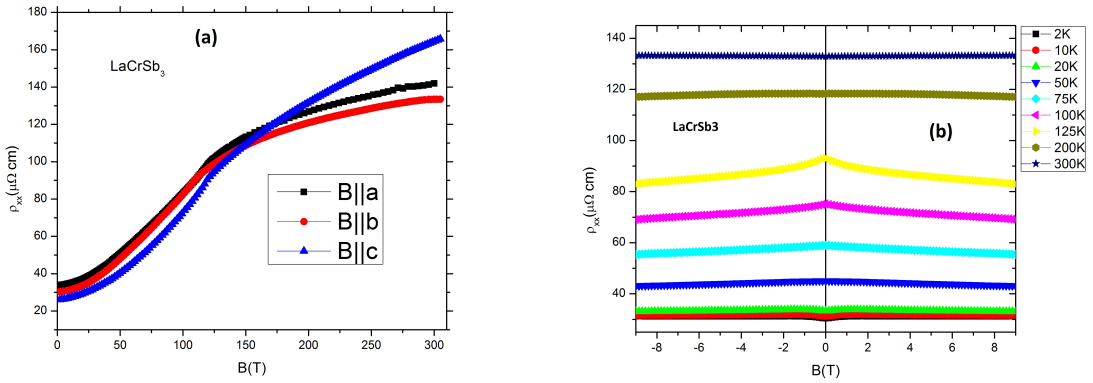

Figure 3.14: Resistivity vs. temperature measurements of $LaCrSb_3$ shows in fig. 3.14a while fig. 3.14b side shows resistivity with applied magnetic field at various temperature.

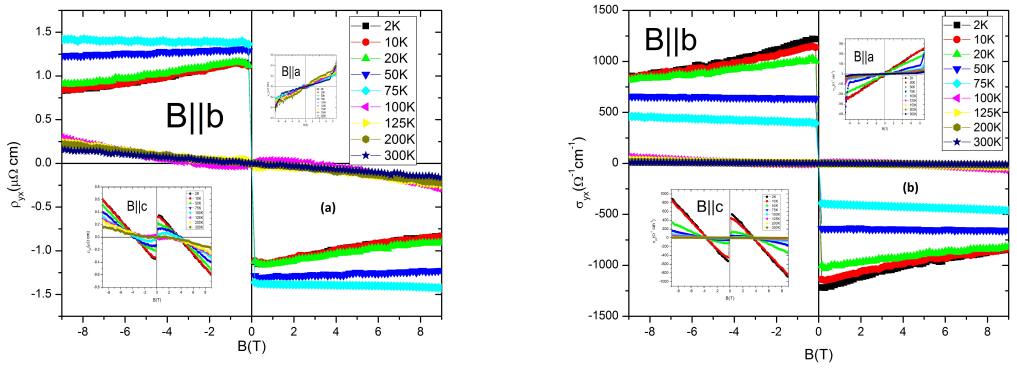

Figure 3.15: Hall resistivity and conductivity of single crystal $LaCrSb_3$ shown in above figure for all a,b,c directions in fig. 3.15a and 3.15b respectively.

$CeCrSb_3$

$CeCrSb_3$ shares many features with $LaCrSb_3$. They are isostructural and same crystallography. The electrical resistivities of both $LaCrSb_3$ and $CeCrSb_3$ were found to have a power law dependence but with different exponents.

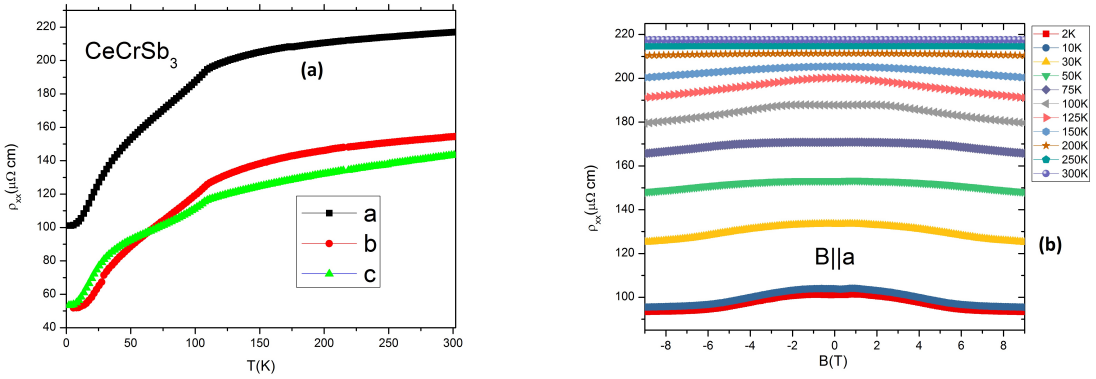

Figure 3.16: Resistivity vs. temperature measurements of $CeCrSb_3$ shows in figure 3.16a while fig. 3.16b shows resistivity with applied magnetic field at various temperature.

As clearly seen from figure 3.17a we observe high anomalous hall in both b and c direction, right figure shows conductivity vs. applied magnetic field B at various temperature calculated from hall measurement using the formula and found that highest conductivity is 1590 $\Omega^{-1}cm^{-1}$, 1380 $\Omega^{-1}cm^{-1}$ along b and c direction respectively.

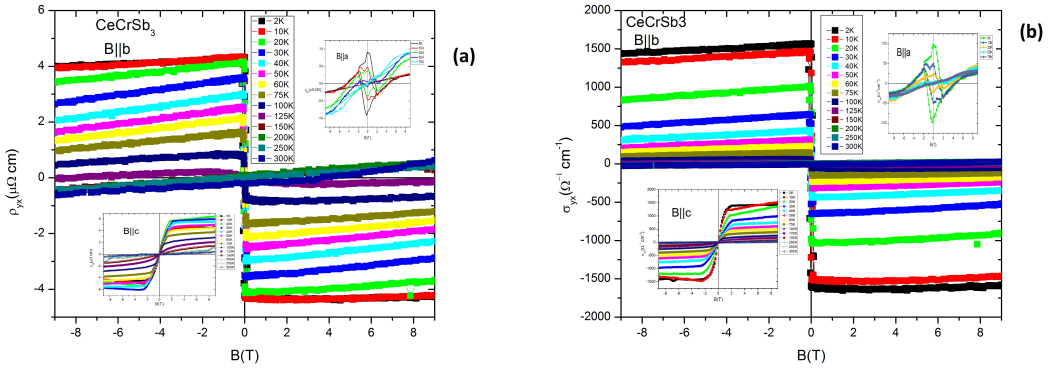

Figure 3.17: Hall resistivity and conductivity of single crystal $CeCrSb_3$ shown for all a,b,c directions in fig.3.17a and 3.17b respectively.

$NdCrSb_3$

The electrical resistivity of single crystals (typically size $1\times1\times3mm^3$) was measured by standard four-probe ac methods with a Quantum Design PPMS between 2K and 300K. After the crystals were cooled in zero fields, the resistivity was measured under

various applied fields. $NdCrSb_3$ exhibits metallic behavior, as shown in the resistivity (Fig. 3.17a)

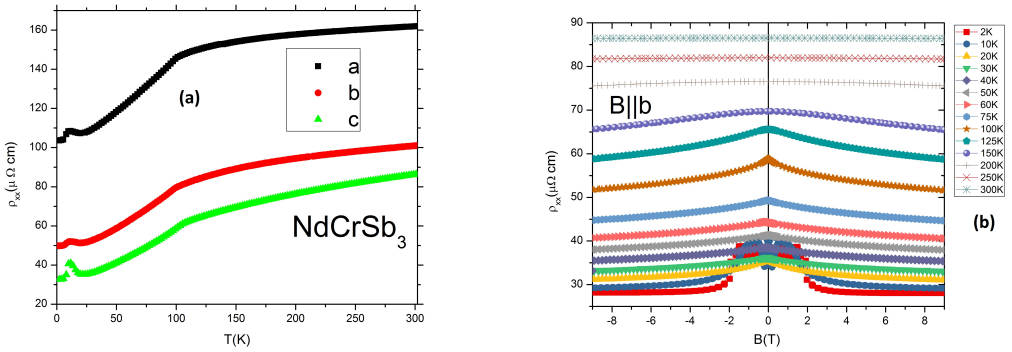

Figure 3.18: Resistivity vs. temperature measurements of $NdCrSb_3$ shows in figure 3.18a while fig. 3.18b shows resistivity with applied magnetic field at various temperature.

As shown in figure 3.19 we observe high anomalous hall in both b and c direction, Right figure shows conductivity vs. applied magnetic field B at various temperature calculated from hall measurement using the formula and found that highest conductivity is 2990 $\Omega^{-1}cm^{-1}$, 880 $\Omega^{-1}cm^{-1}$ along b and c direction respectively. This much value of hall conductivity is highest ever observed value in literature [Guin 19].

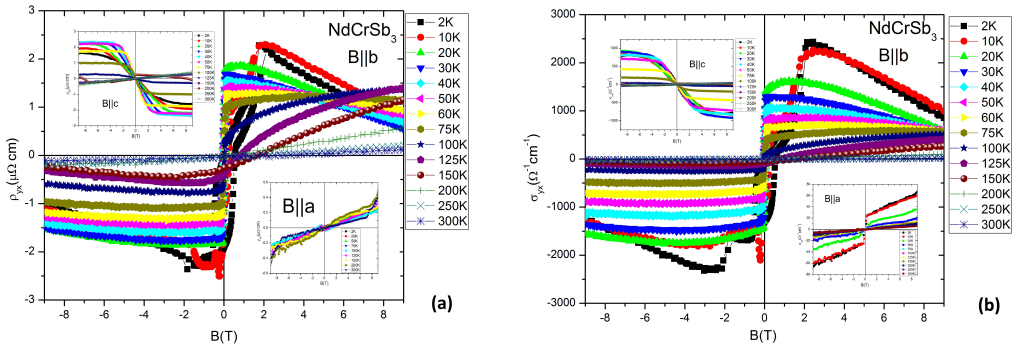

Figure 3.19: Hall resistivity and conductivity of single crystal $NdCrSb_3$ shown for all a,b,c directions in fig. 3.19a and 3.19b respectively.

3.2.6 Calculations

The Hall effect is important to obtain comprehensive information on the external field dependent magnetic texture in a given sample. In general, the measured Hall

resistivity, ρ_{yx} of a topological magnetic material can be expressed by an empirical relation as, $\rho_{yx} = \rho_{y_x}^{N} + \rho_{y_x}^{A} + \rho_{y_x}^{A}$,

Where, the normal Hall effect (NHE) is determined by the relation $\rho_{y_x}^{N} = R_0\mu_0 H$.

The anomalous Hall effect (AHE) in a magnetic material can also be separated and is given by the $\rho_{y_x}^{A} = (\ \alpha\rho_{xx} + S_A\rho_{x_x}^{2})$M, Where α and S_A correspond to the extrinsic contribution from skew scattering and the impurity density independent contributions, respectively. M is the magnetization and ρ_{xx} is the longitudinal resistivity.

Lastly, $\rho_{y_x}^{T}$ is the topological Hall resistivity which arises due to any noncoplanar order of spins. More details were already explained in chapter 1. If anomalous Hall resistivity $\rho_{x_y}^{A}$ and the longitudinal resistivity $\rho_{x_x}^{\alpha}$ were plotted, where α is the scaling power factor $\alpha = 2$ is for the intrinsic KL mechanism and the extrinsic side-jump mechanism and $\alpha = 1$ is for another extrinsic skew-scattering mechanism. We try to extract each part of resistivity as seen from fig. 3.21 we have value of α=2 since $\rho_{y_x}^{2}$ very well fitted into square of $\rho_{x_x}^{2}$. From fig. 3.20 we can again surely confirm this test that we are lying in the intrinsic region of resistivity where high conductance is related to materials band properties.

In fig. 3.20b, the data of other materials were taken from references [Miyasato 07]. Our present result shows a σ_{xx} independent $\sigma_{y_x}^{A}$ below 100K. Our data matches the predictions of the model in which three regimes of the AHE is identified which is already discussed in the introduction of this thesis. $RCrSb_3$ series is located into the intrinsic regime dominated by the Berry-phase curvature, not by the external scattering events.

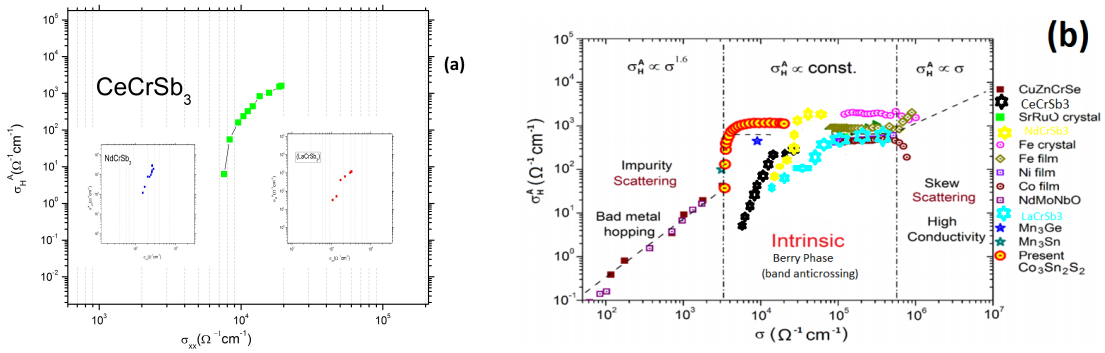

Figure 3.20: Anomalous hall conductivity and longitudinal conductivity for all three single crystals were plotted on log scale in fig. 3.20a while right fig.3.20b shows general trend for class of materials[Miyasato 07].

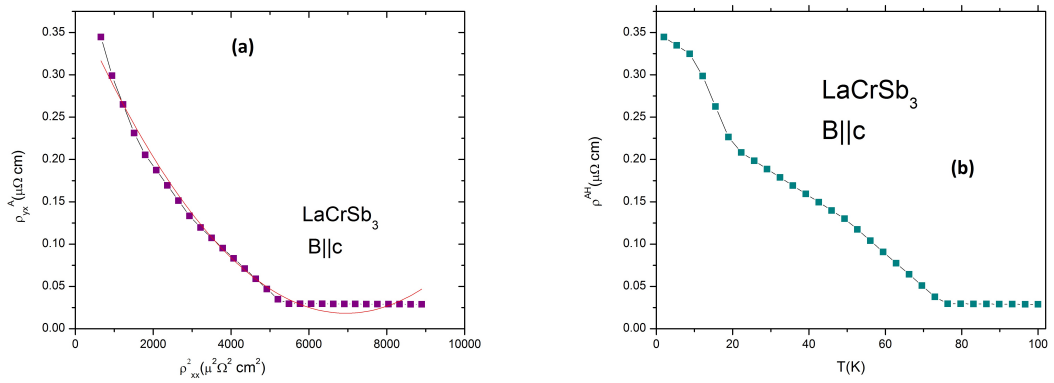

Figure 3.21: anomalous Hall resistivity ρ_{yx}^{A} and the longitudinal resistivity ρ_{xx}^{α} were plotted in fig. 3.21a while fig. 3.21b shows temperature dependence of anomalous Hall resistivity ρ_{yx}^{A}.

If we try to scale our above calculated anomalous hall resistivity with magnetization we left with some non zero part as shown in fig. 3.22a there is a distinct magnetization-independent increase of the Hall effect separate from the normal and anomalous Hall contribution, which is maybe an indication of topological hall effect (THE) in this compound. In contrast to the NHE and AHE, the topological Hall resistivity is maximized in the low external field limit as seen from the fig. 3.22b

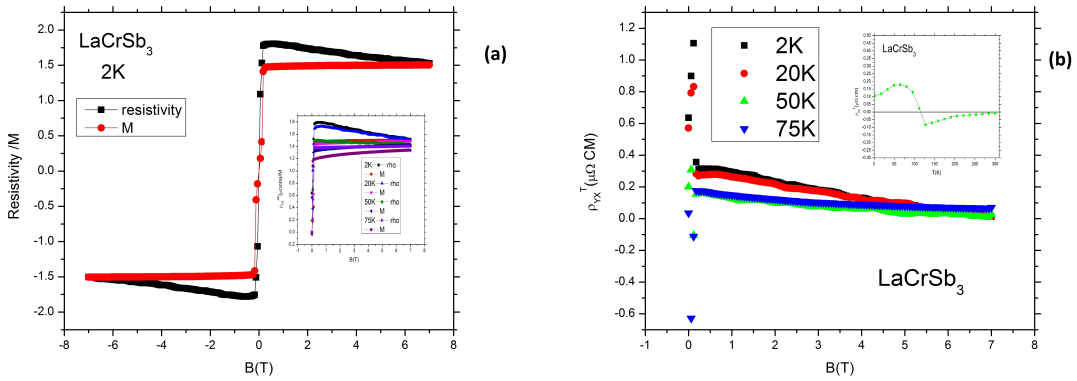

Figure 3.22: (a) shows Topological contribution calculated by scaling anomalous resistivity by magnetization while in fig.3.22b insect shows temperature dependence of topological resistivity.

Chapter 4

Thermal Transport Measurements

Applying a temperature gradient in a magnetic material generates a voltage that is perpendicular to both the heat flow [Rowe 95] called the anomalous Nernst effect (ANE). Initially, it was thought to be proportional to the value of the magnetization for a long time [Nolas 13].In general, the ANE has been predicted to originate from a net Berry curvature of bands near the Fermi level E_F. Subsequently [Liang 17], a large anomalous Nernst thermopower S_{yx}^{A} has recently been observed in topological materials with no net magnetization but large net Berry curvature around E_F [Xiao 06].

4.1 $RCrSb_3$

Nernst thermoelectric measurement was carried out by the one-heater and two-thermometer configuration on a PPMS. All below shown thermal transport data performed within the [010]-plane of the $RCrSb_3$ crystals, with a magnetic field $\mu_0 H$ applied in the [001] direction. A gold plate attached to puck used as the heat sink, two gold-plated copper leads were attached directly to the sample using silver epoxy along the thermal gradient direction for temperature difference measuring, .
As seen from fig. 4.1 at all T, the Nernst signal increases rapidly at low magnetic fields ($\mu_0 H$) and saturates above $\mu_0 H \geq 0.5$T. The Nernst thermopower was estimated as $S_{yx} = L_x E_y/(L_y \Delta T_x)$, where E_Y is transverse electric field, L_x is the distance between two temperature leads, and L_y is the distance between two voltage wires. Similar to the anomalous hall effect(AHE), the anomalous Nernst effect (ANE) of conventional ferromagnets is proportional to the magnetization, that is, $S_{yx}^{A} = N_{yx}^{A} \mu_0 M$ where N_{yx}^{A} is the anomalous Nernst coefficient.

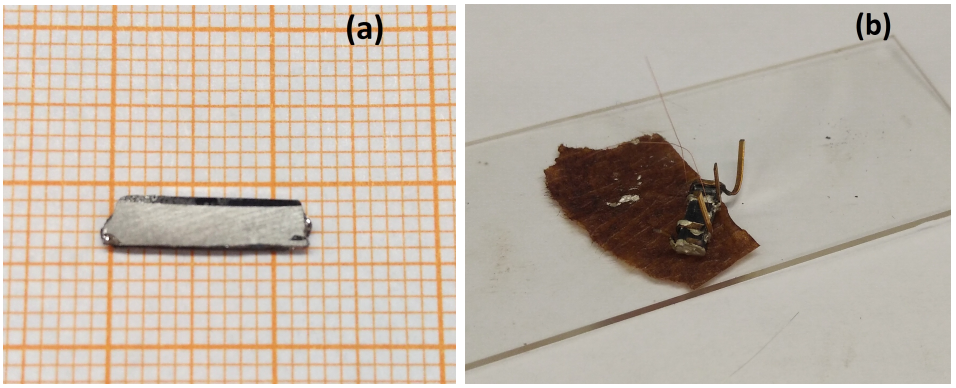

Figure 4.1: Oriented single crystal of $NdCrSb_3$ in fig.4.1a while right 4.1b shows thermal measurement contact made on the sample.

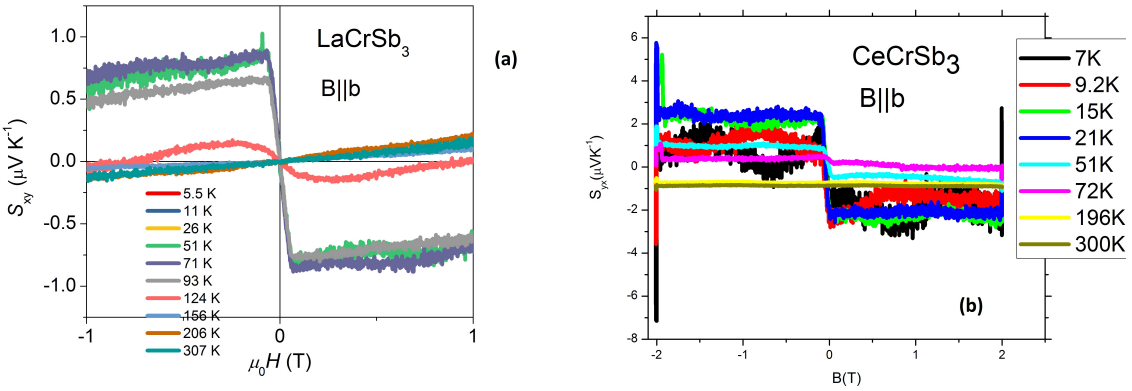

Figure 4.2: The field-dependence of the Nernst thermopower (S_{yx}) for $LaCrSb_3$ and $CeCrSb_3$ at different T in fig. 4.2a, 4.2b respectively.

Bibliography

[Adler 69] Stephen L Adler & William A Bardeen. *Absence of higher-order corrections in the anomalous axial-vector divergence equation*. Physical Review, vol. 182, no. 5, page 1517, 1969.

[Armen 07] G Bradley Armen. *Hall Effect Experiment*. Tennessee, department of Physics and Astronomy, 2007.

[Armitage 18] NP Armitage, EJ Mele & Ashvin Vishwanath. *Weyl and Dirac semimetals in three-dimensional solids*. Reviews of Modern Physics, vol. 90, no. 1, page 015001, 2018.

[Berger 70] L Berger. *Side-jump mechanism for the Hall effect of ferromagnets*. Physical Review B, vol. 2, no. 11, page 4559, 1970.

[Bohm 85] J Bohm. *The history of crystal growth*. Acta Physica Hungarica, vol. 57, no. 3-4, pages 161–178, 1985.

[Cahn 60] John W Cahn. *Theory of crystal growth and interface motion in crystalline materials*. Acta metallurgica, vol. 8, no. 8, pages 554–562, 1960.

[Chang 96] Ming-Che Chang & Qian Niu. *Berry phase, hyperorbits, and the Hofstadter spectrum: Semiclassical dynamics in magnetic Bloch bands*. Physical Review B, vol. 53, no. 11, page 7010, 1996.

[Choi 07] HC Choi, JH Shim, SK Kwon & BI Min. *Electronic structures and magnetic properties of layered compound R Cr Sb 3 (R= La, Yb)*. Journal of applied physics, vol. 101, no. 9, page 09G513, 2007.

[Dhanaraj 10] Govindhan Dhanaraj, Kullaiah Byrappa, Vishwanath Prasad & Michael Dudley. Springer handbook of crystal growth. Springer Science & Business Media, 2010.

[Dingle 52] RB Dingle. *Some magnetic properties of metals II. The influence of collisions on the magnetic behaviour of large systems*. Proceedings of the Royal Society of London. Series A. Mathematical and Physical Sciences, vol. 211, no. 1107, pages 517–525, 1952.

[EDX] https://blog.phenom-world.com/edx-analysis-scanning-electron-microscope-sem.

[Fu 07] Liang Fu, Charles L Kane & Eugene J Mele. *Topological insulators in three dimensions*. Physical review letters, vol. 98, no. 10, page 106803, 2007.

[Granado 01] Eduardo Granado, Jeff Lynn, Damon Jackson & Zack Fisk. *Complex Magnetic Behavior in LaCrSb_3: A Neutron Scattering Study*. In APS Meeting Abstracts, 2001.

[Guin 19] Satya N Guin, Kaustuv Manna, Jonathan Noky, Sarah J Watzman, Chenguang Fu, Nitesh Kumar, Walter Schnelle, Chandra Shekhar, Yan Sun, Johannes Gooth*et al. Anomalous Nernst effect beyond the magnetization scaling relation in the ferromagnetic Heusler compound Co 2 MnGa*. NPG Asia Materials, vol. 11, no. 1, page 16, 2019.

[Hal] http://hyperphysics.phy-astr.gsu.edu/hbase/magnetic/hall.html.

[Haldane 88] F Duncan M Haldane. *Model for a quantum Hall effect without Landau levels: Condensed-matter realization of the" parity anomaly"*. Physical Review Letters, vol. 61, no. 18, page 2015, 1988.

[Hall 79] EH Hall. *On a New Action of the Jla19flet onz Electric Currents.* American Journal of Mathematics, vol. 2, no. 3, pages 287–292, 1879.

[Hall 81] EH Hall. *On the possibility of transvers currents in ferromagnets*. Philos. Mag, vol. 12, pages 157–172, 1881.

[Hammond 01] Christopher Hammond & Christopher Hammond. The basics of cristallography and diffraction, volume 214. Oxford, 2001.

[Inamdar 08] Manjusha Inamdar, A Thamizhavel & S Ramakrishnan. *Anisotropic magnetism in NdCrSb3*. Journal of Physics: Condensed Matter, vol. 20, no. 29, page 295226, 2008.

[Inamdar 09] Manjusha Inamdar, S Ramakrishnan, A Thamizhavel & AK Nigam. *Interplay of 3d and 4f magnetism in RCrSb3*. In Journal of Physics: Conference Series, volume 150, page 042163. IOP Publishing, 2009.

[Jenkins 95] Ron Jenkins. Quantitative x-ray spectrometry. CRC Press, 1995.

[Karplus 54] Robert Karplus & JM Luttinger. *Hall effect in ferromagnetics*. Physical Review, vol. 95, no. 5, page 1154, 1954.

[Kooi 54] Clarence Kooi. *Hall effect in ferromagnetics*. Physical Review, vol. 95, no. 3, page 843, 1954.

[Lau] https://www.slideshare.net/hdghcfgfgftf/x-ray-diffraction-20538757.

[Li 96] DX Li, Y Haga, H Shida, T Suzuki & YS Kwon. *Electrical transport properties of semimetallic GdX single crystals (X= P, As, Sb, and Bi)*. Physical Review B, vol. 54, no. 15, page 10483, 1996.

[Liang 17] Tian Liang, Jingjing Lin, Quinn Gibson, Tong Gao, Max Hirschberger, Minhao Liu, RJ Cava & NP Ong. *Anomalous Nernst effect in the dirac semimetal Cd 3 As 2*. Physical review letters, vol. 118, no. 13, page 136601, 2017.

[Lifshitz 58] IM Lifshitz & LM Kosevich. *On the theory of the Shubnikov-de Haas effect*. Sov. Phys. JETP, vol. 6, pages 67–77, 1958.

[Majorana 37] Ettore Majorana. *Symmetric theory of electron and positron*. Il Nuovo Cimento (1924-1942), vol. 14, no. 4, page 171, 1937.

[Miyasato 07] T Miyasato, N Abe, T Fujii, A Asamitsu, S Onoda, Y Onose, N Nagaosa & Y Tokura. *Crossover behavior of the anomalous Hall effect and anomalous Nernst effect in itinerant ferromagnets*. Physical review letters, vol. 99, no. 8, page 086602, 2007.

[Nolas 13] George S Nolas, Jeffrey Sharp & Julian Goldsmid. Thermoelectrics: basic principles and new materials developments, volume 45. Springer Science & Business Media, 2013.

[Onsager 52] L Onsager. *Interpretation of the de Haas-van Alphen effect*. The London, Edinburgh, and Dublin Philosophical Magazine and Journal of Science, vol. 43, no. 344, pages 1006–1008, 1952.

[Pugh 30] Emerson M Pugh. *Hall effect and the magnetic properties of some ferromagnetic materials*. Physical Review, vol. 36, no. 9, page 1503, 1930.

[Raju 98] NP Raju, John E Greedan, Michael J Ferguson & Arthur Mar. *LaCrSb3: a new itinerant electron ferromagnet with a layered structure*. Chemistry of materials, vol. 10, no. 11, pages 3630–3635, 1998.

[Rowe 95] David Michael Rowe. Crc handbook of thermoelectrics. CRC press, 1995.

[Shim 04] JH Shim & BI Min. *Electronic structures of layered compound LaCrSb3*. Journal of Magnetism and Magnetic Materials, vol. 272, pages E241–E242, 2004.

[Shin 19] Dongbin Shin, Shunsuke A Sato, Hannes Hübener, Umberto De Giovannini, Jeongwoo Kim, Noejung Park & Angel Rubio. *Unraveling materials Berry curvature and Chern numbers from real-time evolution of Bloch states*. Proceedings of the National Academy of Sciences, vol. 116, no. 10, pages 4135–4140, 2019.

[Shoenberg 09] David Shoenberg. Magnetic oscillations in metals. Cambridge university press, 2009.

[Sinitsyn 07] NA Sinitsyn. *Semiclassical theories of the anomalous Hall effect*. Journal of Physics: Condensed Matter, vol. 20, no. 2, page 023201, 2007.

[Tafti 16] FF Tafti, QD Gibson, SK Kushwaha, Neel Haldolaarachchige & RJ Cava. *Resistivity plateau and extreme magnetoresistance in LaSb*. Nature Physics, vol. 12, no. 3, page 272, 2016.

[Weyl 29] Hermann Weyl. *Gravitation and the electron*. Proceedings of the National Academy of Sciences of the United States of America, vol. 15, no. 4, page 323, 1929.

[Xiao 06] Di Xiao, Yugui Yao, Zhong Fang & Qian Niu. *Berry-phase effect in anomalous thermoelectric transport*. Physical review letters, vol. 97, no. 2, page 026603, 2006.

[Yan 17] Binghai Yan & Claudia Felser. *Topological materials: Weyl semimetals*. Annual Review of Condensed Matter Physics, vol. 8, pages 337–354, 2017.